PAPER

# Spontaneous dewetting transition of nanodroplets on nanopillared surface

To cite this article: Shuai Wang *et al* 2020 *Nanotechnology* **31** 225502





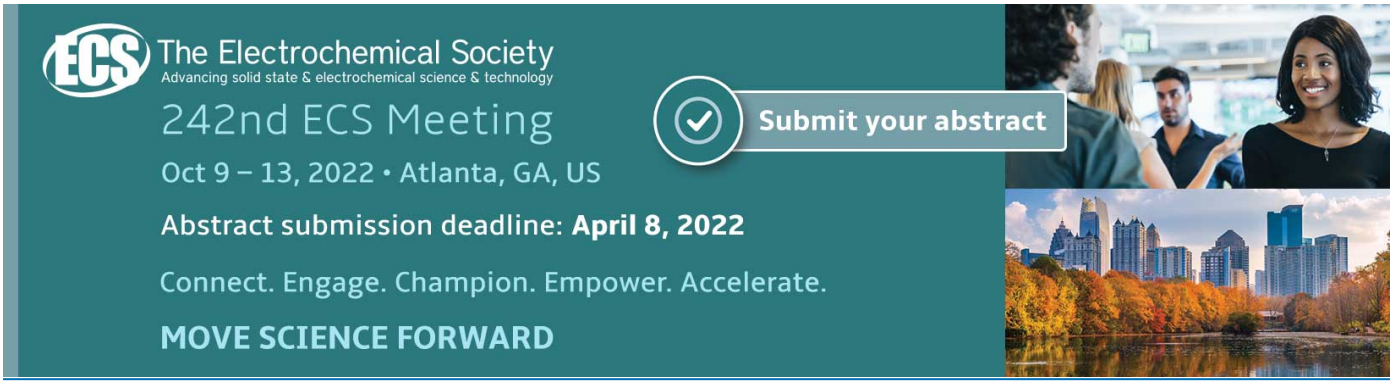

IOP Publishing Nanotechnology
Nanotechnology 31 (2020) 225502 (7pp) https://doi.org/10.1088/1361-6528/ab76f1

# Spontaneous dewetting transition of nanodroplets on nanopillared surface

**Shuai Wang[1,2], Chao Wang[3,5], Zhilong Peng[1,2] and Shaohua Chen[1,2,4,5]**

[1] Institute of Advanced Structure Technology, Beijing Institute of Technology, Beijing, 100081, People's Republic of China
[2] Beijing Key Laboratory of Lightweight Multi-functional Composite Materials and Structures, Beijing Institute of Technology, Beijing, 100081, People's Republic of China
[3] LNM, Institute of Mechanics, Chinese Academy of Sciences, Beijing, 100190, People's Republic of China
[4] State Key Laboratory of Explosion Science and Technology, Beijing Institute of Technology, Beijing 100081, People's Republic of China

E-mail: wangchao@lnm.imech.ac.cn and chenshaohua72@hotmail.com

Received 6 November 2019, revised 27 January 2020
Accepted for publication 17 February 2020
Published 13 March 2020

**Abstract**

The spontaneous dewetting transition (SDT) of nanoscale droplets on the nanopillared surface is studied by molecular dynamics simulations. Three typical SDT modes, i.e. condensing, merging and coalescing with flying droplets are observed, and the underlying physical mechanism is clearly revealed by the potential energy analysis of droplets. We find that there exists a dimensionless parameter of the relative critical volume of droplet $C_{cri}$ which completely controls the SDT of nanodroplets. Furthermore, the $C_{cri}$ remains constant for geometrically similar surfaces, which indicates an intrinsic similarity of nanoscale SDT. The effect of pillar height, diameter and spacing on SDT has also been studied and it is likely to occur on the surface with longer, wider and thicker pillars, as well as pillars with cone-like shape and larger hydrophobicity. These results should be useful for a complete understanding of the nanoscale SDT and shed light on the design of smart superhydrophobic surfaces.

Supplementary material for this article is available online

Keywords: spontaneous dewetting transition, nanoscale droplets, wettability, smart surfaces, molecular dynamics simulation

(Some figures may appear in colour only in the online journal)

## 1. Introduction

Droplets on a rough surface always show sticky Wenzel [1] or slippery Cassie [2] state depending on the intrinsic topological and physicochemical properties of the surface. The two wetting states are convertible under certain conditions [3–6] and the transition from a Wenzel state to a Cassie one is called as dewetting [7, 8]. It has received much attention in recent years due to its critical importance for a wide range of applications, such as heat exchangers [9, 10], anti-icing [11], water harvest [12, 13] and drag reduction [14]. Several methods of external stimuli, like magnetic force [15, 16], electrowetting [17], heating [18], pressure [19] and mechanical vibration [20–22], etc, have been proposed to overcome the energy barrier between the two states to activate dewetting transition. These methods of the externally stimulated dewetting transition have an intrinsic limitation: specific instruments and settings are always required to input external electric, thermal or vibrational energy, which are not always accessible in some practical applications, such as biological systems or micro-/nanoscale lab-on-a-chip systems [23]. So, alternative schemes of the spontaneous dewetting transition (SDT) is highly required, in which, without any external stimuli, the transition is driven only by the spontaneous condensation and coalescence of droplets through the design of nano/microstructures and chemical properties of the surface.

[5] Authors to whom any correspondence should be addressed.

 

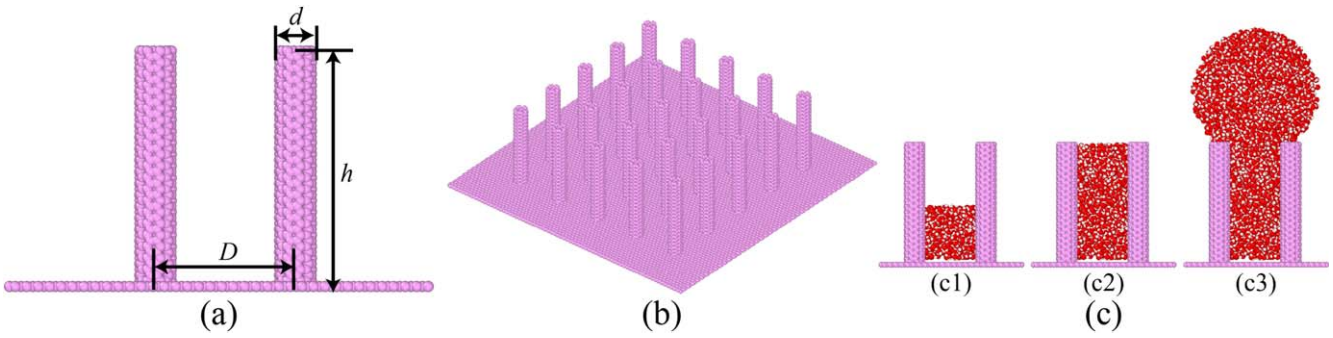


**Figure 1.** Schematic of the SDT system. (a) Front view of a unit of pillared surface with the height $h$, spacing $D$ and diameter $d$; (b) perspective view of the pillared surface; (c) front view of the simulation system with (c1) small, (c2) middle and (c3) large water droplet.

Wang *et al* [24] gave an interesting example from nature about the SDT of condensed microdroplets from the legs of water striders. They found that smaller droplets can stably sink inside arrays of inclined tapered setae on strider's legs, but as droplets grow bigger and bigger from femtoliter to microliter by condensation, they become unstable due to the elastic squeezing of setae arrays and are expelled finally by the recovery force of setae, leading to the robust superhydrophobicity of striders' legs. Lv *et al* [23] conducted an *in situ* observation of the SDT of condensed microdroplets occurring on two-tier nano/micro-structured rigid surfaces. They clearly observed that isolated microdroplets emerge initially at the valley of micropillars, as they grow bigger during condensation, some of them climb to the top of the micropillars unexpectedly to make the transition. They further found three typical modes of the SDT induced by the individual droplet condensation, the merging of two neighboring droplets, and the coalescence induced by a flying droplet from another location. After that, Zhang *et al* [25] found that the SDT is more likely to happen for larger droplets, on the surface with higher wettability and cone-shaped structures through experiments and lattice Boltzmann simulations. Yan *et al* [26] developed a visualization technique to study the coalescence-induced droplet jumping, in which the effect of droplet size, droplet-surface interaction and condensate thermophysical properties are considered. Orejon *et al* [27] fabricated and studied the continuous dropwise condensation on a hierarchical bioinspired lotus leaf metallic surface without the need for a conformal hydrophobic coating. Dong *et al* [28] established theoretical models and numerical methods to predict the wetting state transmission energy barrier.

Although the SDT has been experimentally proved to be feasible, the underlying mechanism and multiple aspects affecting SDT phenomenon is not clearly revealed, limiting the further design of dewetting functional surface. For example, what's the underling mechanism and under which conditions the SDT will be triggered? How does the size and shape of superhydrophobic surface affect the SDT behavior? How to judge and predict whether an SDT will be triggered? For a complete understanding of the SDT phenomenon, it is necessary to study these issues thoroughly, which should shed light on the design of smart superhydrophobic surfaces.

In this paper, we study these issues by applying systematic molecular dynamics (MD) simulations. The rest of this article is organized as follows. The numerical model of nanoscale droplet-pillared surface is established first. Then, the underlying mechanism of the nanoscale SDT is unveiled and an interesting similarity is given accordingly. Furthermore, the effect of geometric parameters of the height, diameter, spacing and shape of nanopillars, the substrate wettability on the SDT is examined carefully in the following section. The results are summarized at the end of the paper.

## 2. Numerical model and methodology

Figure 1(a) shows the structure unit of the nano-pillared surface with geometrical settings of height ($h$), diameter ($d$) and spacing ($D$) of pillars simulated by single-walled carbon nanotubes (SWCNTs). The pillared surface is then obtained by periodically extending the structure unit on a single-layer graphene sheet as shown in figure 1(b). Three typical states of small, mediate and large droplet volume $V$ are depicted in figure 1(c).

To enable SDT, the settings of $h$, $d$ and $D$ for pillared surface in all simulations should be chosen carefully to meet equation 1 which is the criterion of Wenzel-to-Cassie transition [4, 29] for the extreme case that the pillared surface is invaded by plenty of liquid as shown in figure S1 of the supporting information, which is available online at stacks.iop.org/NANO/31/225502/mmedia.

$$\theta_{\mathrm{cri}} < \theta, \tag{1}$$

where $\theta_{\mathrm{cri}}$ and $\theta$ are the critical contact angle and the contact angle, $\theta$ is determined by the physicochemical property of materials; $\theta_{\mathrm{cri}}$ is determined by the structural properties of the surface and can be calculated by $\cos\theta_{\mathrm{cri}} = \dfrac{f-1}{r-f}$, where $r = \dfrac{\pi d^2}{4D^2}$ and $f = 1 + \dfrac{\pi dh}{D^2}$ are roughness factor and surface fraction occupied by pillars.

The AIREBO potential is adopted to describe the C–C interaction in SWCNTs and graphene. The simple point charge-extended (SPC/E) model [30, 31] with the SHAKE algorithm [32] is used to describe the water droplet, and the long-range Coulomb interactions in water droplet are

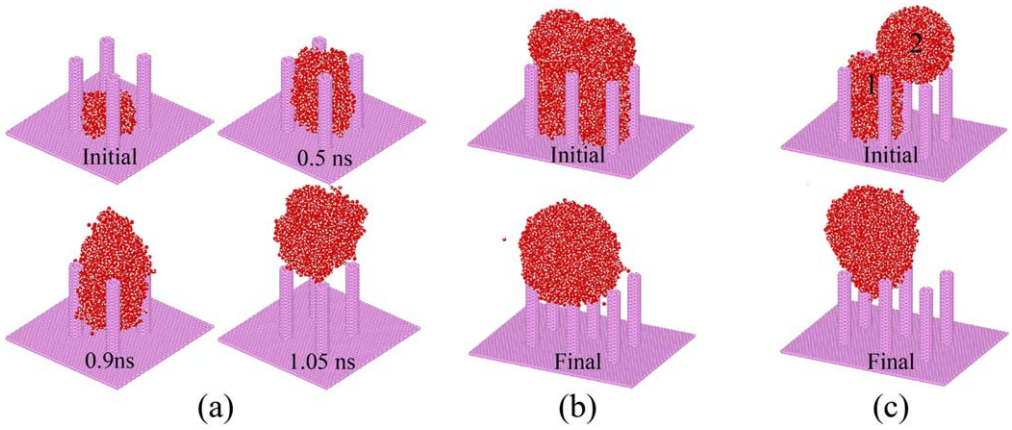


**Figure 2.** The three modes of the SDT for nanodroplets induced by (a) Mode I: the droplet condensation; (b) Mode II: the merging of two neighboring droplets; (c) Mode III: the coalescence induced by a flying droplet. $D = 3$ nm, $d = 0.68$ nm, $h = 5$ nm for all cases.

computed using the particle–particle particle-mesh algorithm [33]. The interactions between oxygen atoms of water and carbon atoms of SWCNTs/graphene are described by the Lennard-Jones potential $\varphi(r) = 4\varepsilon[(\sigma/r)^{12}–(\sigma/r)^{6}]$, with the equilibrium distance $\sigma$ of 0.319 nm and the well depth $\varepsilon$ of 1.95 meV. The $\sigma$ and $\varepsilon$ are tuned directly to study the effect of surface hydrophobicity of pillars and substrate qualitatively, which has been widely used to study the movement of droplet with different wettability [34–36]. The contact angle of nanopillars is set to be 138° and zero contact angle hysteresis is adopted in this model as done in the [35]. In experiments, the large hydrophobicity of graphene material can be achieved through charge carrier density [37], oxygen-containing functional groups [38] or even hierarchical structures [39], despite the differences of scales, the wetting property of pillars in experiments can also be simulated by fitting the parameters of potential function. A NVT ensemble with Nosé–Hoover thermostats [40] is used to keep the temperature of water droplet at 300 K, and the carbon atom keep still during the simulation to depict a rigid pillared surface. All simulations are performed using the open-source large-scale atomic/molecular massively parallel simulator software [41]. All figures and movies are made by the open source software Ovito [42].

## 3. SDT and influencing factors

### *3.1. Transition modes and underlying mechanism*

Figure 2(a) shows the SDT of a nanodroplet during condensation. Initially, a small droplet containing 516 water molecules condenses and stays in the valley of pillars. Due to the condensation which is simulated by adding water molecules gradually near droplet surface, the droplet grows bigger and bigger and fills the valley gradually as shown in the snapshot at 0.5 ns. As the droplet grows to a certain size, an SDT is triggered suddenly at ~0.9 ns and the droplet climbs to the pillars top in a very short interval of 0.9–1.05 ns. After that, the droplet remains Cassie state at the top of the pillared surface (see movie S1 in the supporting information for the whole process). The SDT can also be triggered by the merging of two neighboring droplets. As shown in figure 2(b) and movie S2, as the two neighboring droplets grow to a certain size, they merge into a large one and climb up to the top of pillared surface. To verify that the SDT is triggered by droplets merging, we separate them initially and let them grow independently to the same size, the SDT is not observed any more as shown in figure S2f and movie S3 of the supporting information. Besides, the SDT can also be triggered by the coalescence induced by a flying droplet. As shown in figure 2(c) and movie S4, a droplet marked as '2' flies on the surface from another location, and rans into the Sunk droplet marked as '1', then the Sunk droplet is pulled up from the groove and merges with the flying one. These three modes of SDT is consistent with 'Mode I', 'Mode II' and 'Mode III' classified by Lv *et al* [23] in experiment, initiating the reliability of our simulation.

To clarify the underlying mechanism of the nanoscale SDT as simulated in figure 2, we calculate the potential energy of a nano-droplet fixed at different position along the $z$-axis in the pillared valley. For a smaller droplet, as shown in figure 3(a), the nonlinear potential energy is dependent on droplet position and the smallest value of potential energy can only be observed when droplet lie at the bottom of the valley, i.e. in the Wenzel state as the first inset in figure 3(a). There is a large energy barrier ($E_{W2C}$) between the Wenzel and Cassie state, which makes the Wenzel state more stable and prevent the spontaneous transition to a Cassie state for smaller droplets. However, the opposite is true for larger droplets, as shown in figure 3(b), the potential energy of a larger droplet in Wenzel state (the first inset) is larger than that in the Cassie one (the second inset), which leads to the SDT as observed in figure 2. It indicates that the droplet volume is a key factor dominating its wetting state in pillared valley, and there should be a critical volume $V_{cri}$, above which, the nanoscale SDT occurs. The similar conclusion has been reported for the SDT of microscale droplets using the lattice Boltzmann simulations in the [25].

### *3.2. The similarity of nanoscale SDT*

To further study the effect of droplet volume on the nanoscale SDT quantitatively, a dimensionless parameter of relative

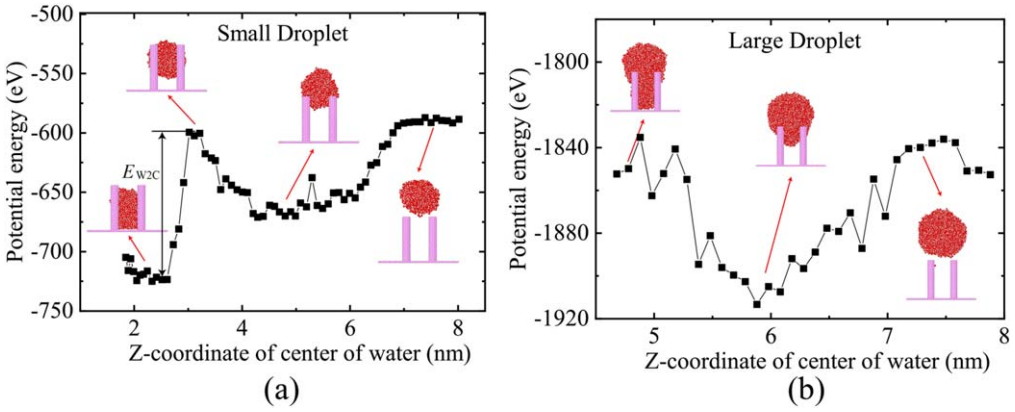


**Figure 3.** Variation of potential energy as a function of *Z*-coordinate of mass center for a (a) small and (b) large droplet. $D = 3$ nm, $d = 0.68$ nm, $h = 5$ nm for both cases.

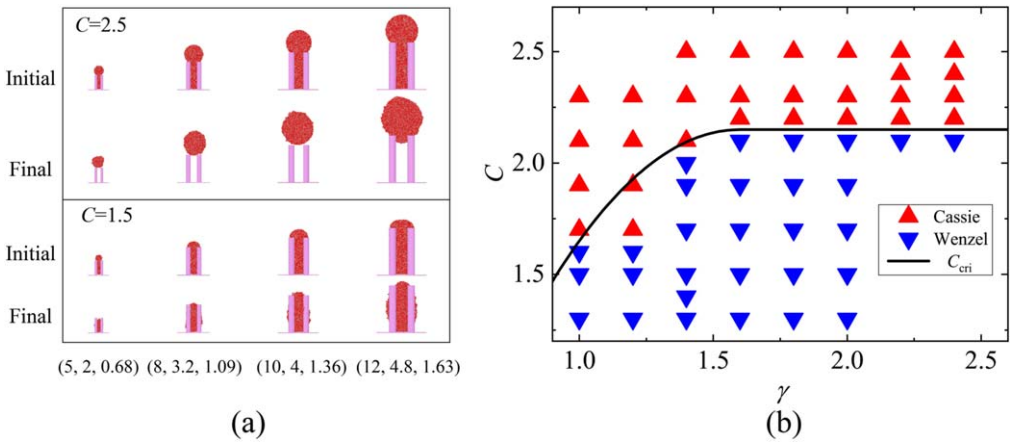


**Figure 4.** The similarity of the nanoscale SDT. (a) Typical examples of SDT systems with different relative volume *C* but similar pillared surface. The geometrical parameters of *h*, *D* and *d* with the unit of nanometer are shown below the corresponding graph; (b) the SDT results for droplets with a series of relative volume *C* on similar pillared surface characterized by variable scale factor $\gamma$, where $\gamma = h/h_0 = D/D_0 = d/d_0$, $h_0$, $D_0$ and $d_0$ are 5, 2 and 0.68 nm, respectively.

volume is defined as $C = V/V_0$, where $V_0$ and $V$ are the volume when droplet is just full of pillar valley as shown in figure 1c2 and the current one, respectively. Similarly, the relative critical volume $C_{cri}$ is defined as $C_{cri} = V_{cri}/V_0$, where $V_{cri}$ is the critical droplet volume discussed above. We study the SDT for the droplet with different volume $C$ on eight similar surfaces with the geometrical parameters of $h$, $D$ and $d$ increased proportionally with the scale factor $\gamma$ in the range of 1–2.4, ($\gamma = h/h_0 = D/D_0 = d/d_0$, $h_0$, $D_0$ and $d_0$ are 5, 2 and 0.68 nm, respectively). For a large $\gamma > 2.4$, it will cost too much computational time to conduct simulations because the number of atoms in the system increases exponentially with $\gamma$. Figure 4(a) gives the SDT of smaller/bigger droplets on four typical similar surfaces with the scale factor $\gamma = 1$, 1.6, 2.0, and 2.4, respectively. The SDT occurs for bigger droplets with $C = 2.5$ on the four similar surfaces as shown in the top row in figure 4(a) while it fails for the smaller droplet with $C = 1.5$ as shown in the bottom row. Figure 4(b) shows all simulation results that the red triangles indicate successful SDT cases as the top row in figure 4(a) while the blue ones indicate unsuccessful SDT as the examples in the bottom row in figure 4(a). It is reasonable that the relative critical volume $C_{cri}$ of droplets falls in the range between the 'red' and 'blue' ones as indicated by the solid line in figure 4(b). Interestingly, the $C_{cri}$ approaches to a constant with an increased $\gamma$ as the solid line in figure 4(b), i.e. the nanoscale SDT has an intrinsic similarity, which is also independent on the initial geometric parameters ($h_0$, $D_0$ and $d_0$) chosen in simulations as discussed in figure S5 in supporting information. The $C_{cri}$ deviates a little from the convergence for the system with smaller $\gamma$, this is because, the volume of the gap between nanopillars and droplets is comparable to the volume of droplet for the system with smaller $\gamma$, while it is negligible for the system with larger $\gamma$. A detailed explanation can be found in the supporting information.

### *3.3. The effect of pillar height, diameter and spacing*

Figure 5(a) shows the $C_{cri}$ as a function of $h$ for $D = 3$ nm and $d = 0.68$ nm. The $C_{cri}$ decreases nonlinearly with increased $h$, showing that the SDT of a droplet can be triggered more easily on the surface with higher nanopillars. To test this point, we simulate the SDT of the two pillar-droplet systems with the same $C$ and different $h$ of 3 and 5 nm, as the two insets shown in figure 5(a), the SDT only occurs in the system with higher pillars of 5 nm (the red triangle), where the $C > C_{cri}$ is achieved. It is explained as blow: the droplet in the surface of higher pillars

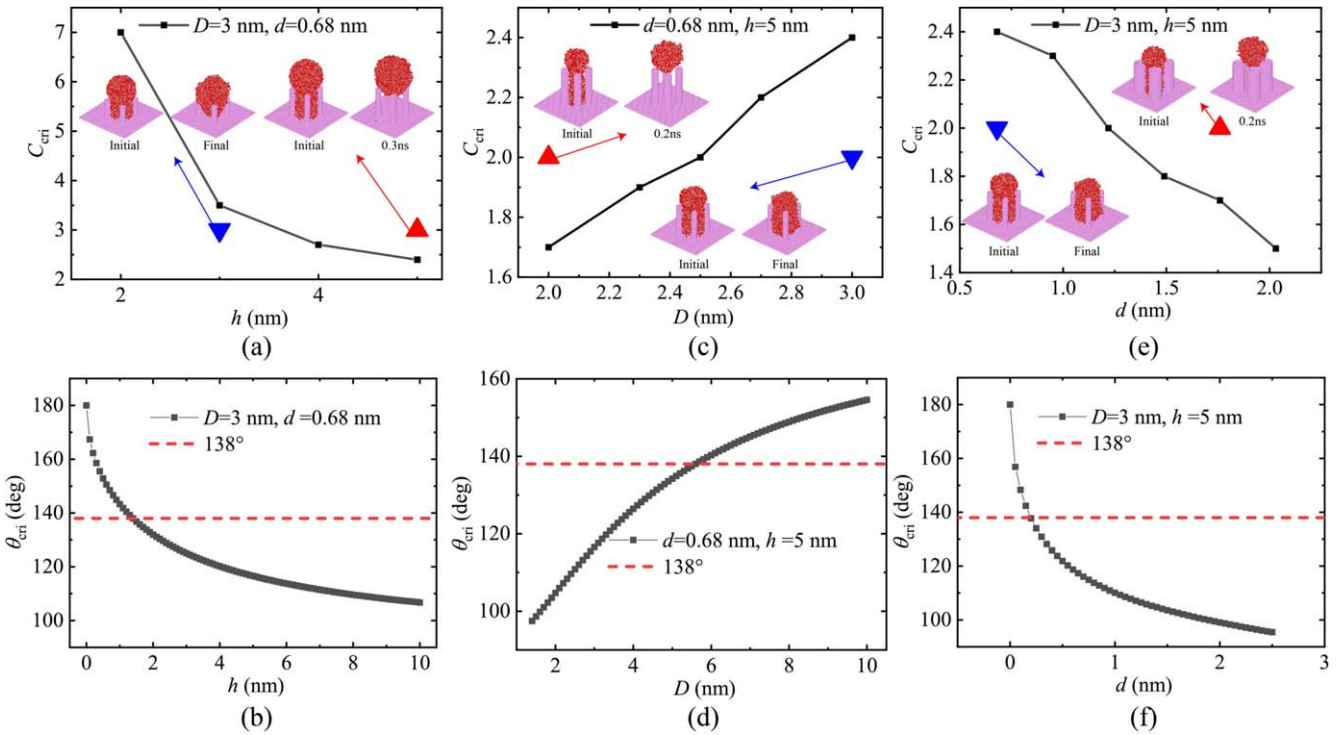


**Figure 5.** The relative critical volume $C_{cir}$ and the critical contact angle $\theta_{cir}$ as a function of (a), (b) pillar height $h$, (c), (d) spacing $D$ and (e), (f) diameter $d$.

exhibits lathy state which has more surface energy than that in an approximately spherical state in a short-pillar surface, hence, it is more likely to move out of the valley to be spherical state to release the excess surface energy. It is noted that the $C_{cri}$ would increase to a high value of 7 as $h$ decreases to 2 nm, indicating that the SDT can occur only for much large droplets. We also test in our simulations that the droplet will always be in Wenzel state no matter how large the droplet is if $h$ further decreases to 1 nm. This is consistent with the prediction by the criterion of Wenzel-to-Cassie transition according to equation 1, as shown in figure 5(b), the critical contact angle $\theta_{cri}$ increases greatly as $h$ decreases and it will be larger than $\theta$ (138° as marked by the red dotted line) if $h$ is lower than 1.40 nm, as a result, the SDT cannot be triggered no matter how large the droplet is. Meanwhile, the $h$ cannot be too large as well, otherwise, the condensed droplet will move to the neighboring groove rather than jump to the top as shown in figure S6.

Figure 5(c) shows the $C_{cri}$ as a function of $D$. The $C_{cri}$ decreases with the decrease of $D$, indicating that the SDT is more likely to be triggered for droplets on the surface having smaller gap between neighboring pillars. We also simulate the dewetting behavior of the two pillar-droplet systems with the same $C = 2$, $d = 0.68$ nm and $h = 5$ nm, but different $D$ of 2 and 3 nm, respectively. As shown in the two insets in figure 5(c), the SDT only occurs in the system with $D = 2$ nm (the red triangle) due to the condition of $C > C_{cri}$ is satisfied. With an increasing $D$, the contact area of solid-liquid interface increases, which results in larger potential energy barrier need to be overcome for the dewetting transition. Figure 5(d) shows that the critical contact angle $\theta_{cri}$ will be larger than $\theta$ if $D$ is larger than 5.59 nm according to the criterion of Wenzel-to-Cassie transition, in which the SDT cannot be triggered any more no matter how large the droplet is.

Figure 5(e) shows the $C_{cri}$ as a function of $d$. The $C_{cri}$ decreases with an increase of $d$, indicating that the SDT is more likely to occur on the surface with wider pillars for given $h$ and $D$. To test this point, we simulate the dewetting behavior of the two pillar-droplet systems with the same $C = 2$, $D = 3$ nm and $h = 5$ nm, but different $d$ of 0.68 and 1.76 nm, respectively. As shown in the two insets in figure 5(e), the dewetting transition can only occur in the system with wider pillars of 1.76 nm (the red triangle) due to the condition of $C > C_{cri}$ is only satisfied in this case. Figure 5(f) shows that the critical contact angle $\theta_{cri}$ increases greatly as pillar diameter $d$ decreases and $\theta_{cri}$ will be larger than $\theta$ if $d$ is lower than 0.20 nm, theoretically. In fact, the diameter of nanopillars in experiments is always larger than 0.20 nm, so this condition can always be satisfied in real applications.

Figure 6(a) shows the $C_{cri}$ as a function of the substrate hydrophobicity measured through contact angle. The $C_{cri}$ decreases sharply with increasing contact angle, which indicates that the SDT prefers to occur on the surface having higher hydrophobicity. We simulate the dewetting behavior of the two pillar-droplet systems with the same settings of $C$, $D$, $h$ and $d$, but different contact angle of 121° and 138°, respectively. As the insets shown in figure 6(a), only the droplet with the higher contact angle (138°) moves to the top of the pillar to make the transition. It is qualitatively consistent with the experimental finding [25] that the SDT of microscale droplets is more likely to happen on the surface with higher wettability.

Figure 6(b) shows the $C_{cri}$ as a function of $D$ for the surface having three shapes of cone-like, inverted cone-like and columnar nanopillars. The $C_{cri}$ increases with $D$ for both cone-like and columnar structure surface, and for a given $D$, the $C_{cri}$

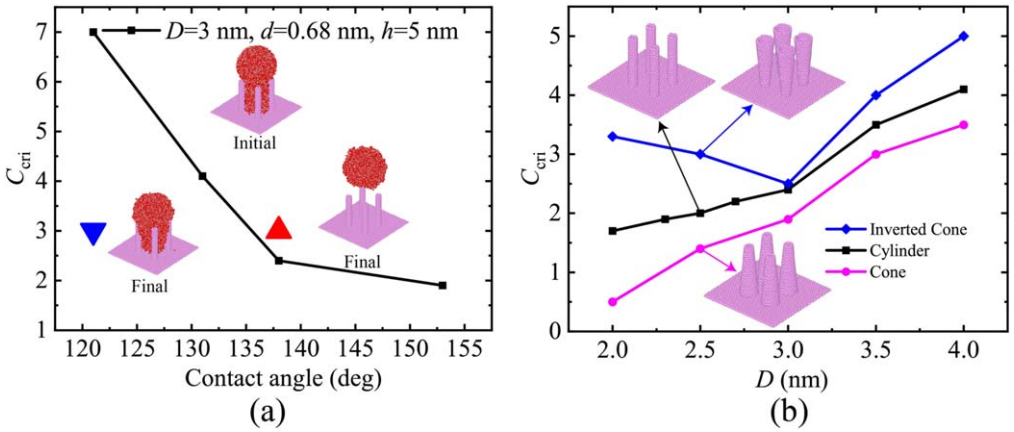


**Figure 6.** The effect of wettability and pillar shape on SDT. (a) The $C_{cri}$ as a function of contact angle. (b) The $C_{cri}$ as a function of $D$ for three pillar shapes of cone-like, inverted cone-like and columnar nanopillars. $D = 3$ nm, $d = 0.68$ nm, $h = 5$ nm for all pillared surface. $D = 2$ nm and $h = 5$ nm for both cone-like and inverted cone-like, while the minimum and maximum diameter are 0.68 and 1.36 nm, respectively.

for cone-like structure surface is a little smaller than that for a columnar one. Furthermore, the $C_{cri}$ is always larger than 1 for columnar structure surface while it could be smaller than 1 for a cone-like surface, which proves that the cone-like structure surface is an optimal choice for SDT. By contrast, the inverted cone-like structure surface is not optimal because the corresponding $C_{cri}$ is larger compared other two kinds of structures.

## 4. Conclusions

In this paper, we study the SDT of nanoscale water droplets on the nano-pillared hydrophobic surface driven by the spontaneous droplet condensation and coalescence through systematic MD simulations. It is found that the nanoscale SDT can be triggered by three modes: the individual droplet condensation, the merging of neighboring droplets and the coalescence induced by a flying droplet from another location, which are similar to the SDT of microscale droplets found in experiments by Lv *et al* [23]. By the analysis of the potential energy of the droplet with different size in pillared valley, we found that it is the droplet volume that dominates the wetting state, i.e. smaller droplets prefer to be in Wenzel state while larger droplets are more likely to be in Cassie one. There is a relative critical volume $C_{cri}$, and the SDT occurs only when the condition $C > C_{cri}$ is achieved. Furthermore, it is found that the SDT has an intrinsic similarity that the $C_{cri}$ remains unchanged as the geometrical parameters of pillar height $h$, diameter $d$ and spacing $D$ increased proportionally. Using the two crucial parameters, i.e. critical contact angle $\theta_{cri}$ and relative critical volume $C_{cri}$, we study the effect of the geometrical settings of the substrate, and found that both parameters increases with the increasing $D$ but decreases with the increasing $h$ and $d$, indicating that SDT is more likely to occur on the pillared surface with higher height, larger diameter and smaller spacing. The relative critical volume $C_{cri}$ decreases with the increasing contact angle of surface. The relative critical volume $C_{cri}$ increases with the spacing $D$ for cone-like structure surface, for a given $D$, the $C_{cri}$ for cone-like structure surface is a little smaller than that for a columnar one, which indicates that the cone-like structure surface is an optimal choice for SDT. By contrast, the inverted cone-like structure surface is not the optimal choice due to the larger corresponding $C_{cri}$ relative to other two kinds of structures. The results should be benefit for a complete understanding of the nanoscale SDT and shed light on the design of smart superhydrophobic surfaces.

## Acknowledgments

The work reported here is supported by NSFC through Grants #11872114, #11532013, #11972348, #11602270.

## Conflicts of interest

There are no conflicts of interest to declare.

## Author contributions

SHC and CW conceived the original idea, designed and supervised the simulations. SW formulated the numerical model, conducted all simulations and drafted the paper. CW revised the manuscript. All authors reviewed and contributed to the paper.

## ORCID iDs

Chao Wang https://orcid.org/0000-0002-3234-6917
Shaohua Chen https://orcid.org/0000-0002-5277-453X

## References

[1] Wenzel R N 1936 Resistance of solid surfaces to wetting by water *Ind. Eng. Chem.* **28** 988–94
[2] Cassie A and Baxter S 1944 Wettability of porous surfaces *Trans. Faraday Soc.* **40** 546–51

[3] Miljkovic N, Enright R and Wang E N 2012 Effect of droplet morphology on growth dynamics and heat transfer during condensation on superhydrophobic nanostructured surfaces *ACS Nano* **6** 1776–85

[4] Lafuma A and Quéré D 2003 Superhydrophobic states *Nat. Mater.* **2** 457–60

[5] Lv P, Xue Y, Shi Y, Lin H and Duan H 2014 Metastable states and wetting transition of submerged superhydrophobic structures *Phys. Rev. Lett.* **112** 196101

[6] Cao Z, Stevens M J, Carrillo J-M Y and Dobrynin A V 2015 Adhesion and wetting of soft nanoparticles on textured surfaces: transition between wenzel and cassie-baxter states *Langmuir* **31** 1693–703

[7] Boreyko J B and Collier C P 2013 Dewetting transitions on superhydrophobic surfaces: when are wenzel drops reversible? *J. Phys. Chem.* C **117** 18084–90

[8] Boreyko J B, Baker C H, Poley C R and Chen C H 2011 Wetting and dewetting transitions on hierarchical superhydrophobic surfaces *Langmuir* **27** 7502–9

[9] Tian J, Zhu J, Guo H Y, Li J, Feng X Q and Gao X 2014 Efficient self-propelling of small-scale condensed microdrops by closely packed ZnO nanoneedles *J. Phys. Chem. Lett.* **5** 2084

[10] Daniel S, Chaudhury M K and Chen J C 2001 Fast drop movements resulting from the phase change on a gradient surface *Science* **291** 633

[11] Kim P, Wong T-S, Alvarenga J, Kreder M J, Adorno-Martinez W E and Aizenberg J 2012 Liquid-infused nanostructured surfaces with extreme anti-ice and anti-frost performance *ACS Nano* **6** 6569–77

[12] Zhai L, Berg M C, Cebeci F C, Kim Y, Milwid J M, Rubner M F and Cohen R E 2006 Patterned superhydrophobic surfaces: toward a synthetic mimic of the namib desert beetle *Nano Lett.* **6** 1213–7

[13] Garrod R P, Harris L G, Schofield W C, Mcgettrick J, Ward L J, Teare D O and Badyal J P 2007 Mimicking a stenocara beetle's back for microcondensation using plasmachemical patterned superhydrophobic-superhydrophilic surfaces *Langmuir* **23** 689–93

[14] Srinivasan S, Kleingartner J A, Gilbert J B, Cohen R E, Milne A J and McKinley G H 2015 Sustainable drag reduction in turbulent taylor-couette flows by depositing sprayable superhydrophobic surfaces *Phys. Rev. Lett.* **114** 014501

[15] Cheng Z, Lai H, Zhang N, Sun K and Jiang L 2012 Magnetically induced reversible transition between cassie and wenzel states of superparamagnetic microdroplets on highly hydrophobic silicon surface *J. Phys. Chem.* C **116** 18796–802

[16] Yang C, Wu L and Li G 2018 Magnetically responsive superhydrophobic surface: *in situ* reversible switching of water droplet wettability and adhesion for droplet manipulation *ACS Appl. Mater. Interfaces* **10** 20150–8

[17] Kumari N and Garimella S V 2011 Electrowetting-induced dewetting transitions on superhydrophobic surfaces *Langmuir* **27** 10342–6

[18] Liu G, Fu L, Rode A V and Craig V S 2011 Water droplet motion control on superhydrophobic surfaces: exploiting the wenzel-to-cassie transition *Langmuir* **27** 12769–70

[19] Verho T, Korhonen J T, Sainiemi L, Jokinen V, Bower C, Franze K, Franssila S, Andrew P, Ikkala O and Ras R H 2012 Reversible switching between superhydrophobic states on a hierarchically structured surface *Proc. Natl Acad. Sci. USA* **109** 10210–3

[20] Boreyko J B and Chen C H 2009 Restoring superhydrophobicity of lotus leaves with vibration-induced dewetting *Phys. Rev. Lett.* **103** 174502

[21] Li Y P, Li X Y, Zhu X P, Lei M K and Lakhtakia A 2018 Polymer surface textured with nanowire bundles to repel high-speed water drops *Langmuir* **34** 5871–9

[22] Moradi M, Rahimian M H and Chini S F 2019 Numerical investigation of vibration-induced droplet shedding on smooth surfaces with large contact angles *Phys. Rev.* E **100** 023105

[23] Lv C, Hao P, Zhang X and He F 2015 Dewetting transitions of dropwise condensation on nanotexture-enhanced superhydrophobic surfaces *ACS Nano* **9** 12311–9

[24] Wang Q, Yao X, Liu H, Quéré D and Jiang L 2015 Self-removal of condensed water on the legs of water striders *Proc. Natl Acad. Sci. USA* **112** 9247–52

[25] Zhang B, Chen X, Dobnikar J, Wang Z and Zhang X 2016 Spontaneous wenzel to cassie dewetting transition on structured surfaces *Phys. Rev. Fluids* **1** 073904

[26] Yan X, Zhang L, Sett S, Feng L, Zhao C, Huang Z, Vahabi H, Kota A K, Chen F and Miljkovic N 2019 Droplet jumping: effects of droplet size, surface structure, pinning, and liquid properties *ACS Nano* **13** 1309–23

[27] Orejon D, Askounis A, Takata Y and Attinger D 2019 Dropwise condensation on multiscale bioinspired metallic surfaces with nanofeatures *ACS Appl. Mater. Interfaces* **11** 24735–50

[28] Dong J, Jin Y, Dong H, Liu J and Ye S 2018 Numerical study for a large-volume droplet on the dual-rough surface: apparent contact angle, contact angle hysteresis, and transition barrier *Langmuir* **34** 8119–27

[29] Quéré D 2008 Wetting and roughness *Annu. Rev. Mater. Res.* **38** 71–99

[30] González M A and Abascal J L 2010 The shear viscosity of rigid water models *J. Chem. Phys.* **132** 096101

[31] Berendsen H J C, Grigera J R and Straatsma T P 1987 The missing term in effective pair potentials *J. Phys. Chem.* **91** 6269–71

[32] Ryckaert J P, Ciccotti G and Berendsen H J C 1977 Numerical integration of the cartesian equations of motion of a system with constraints: molecular dynamics of n-alkanes *J. Comput. Phys.* **23** 327–41

[33] Hockney R W and Eastwood J W 1988 *Computer Simulation Using Particles* (Boca Raton, FL: CRC Press)

[34] Wang S, Wang C, Peng Z and Chen S 2019 Moving behavior of nanodroplets on wedge-shaped functional surfaces *J. Phys. Chem.* C **123** 1798–805

[35] Lv C J, Chen C, Chuang Y-C, Tseng F-G, Yin Y J, Grey F and Zheng Q S 2014 Substrate curvature gradient drives rapid droplet motion *Phys. Rev. Lett.* **113** 026101

[36] Liu Q and Xu B 2015 Actuating water droplets on graphene via surface wettability gradients *Langmuir* **31** 9070–5

[37] Ashraf A, Wu Y, Wang M C, Yong K, Sun T, Jing Y, Haasch R T, Aluru N R and Nam S 2016 Doping-induced tunable wettability and adhesion of graphene *Nano Lett.* **16** 4708–12

[38] Wei N, Lv C and Xu Z 2014 Wetting of graphene oxide: a molecular dynamics study *Langmuir* **30** 3572–2578

[39] Zheng Q S, Lv C J, Hao P F and Sheridan J 2010 Small is beautiful, and dry *Sci. China Phys., Mech. Astron.* **53** 2245–59

[40] Shinoda W, Shiga M and Mikami M 2004 Rapid estimation of elastic constants by molecular dynamics simulation under constant stress *Phys. Rev.* B **69** 134103

[41] Plimpton S 1993 Fast parallel algorithms for short-range molecular dynamics *J. Comput. Phys.* **117** 1–19

[42] Stukowski A 2010 Visualization and analysis of atomistic simulation data with OVITO–the Open Visualization Tool *Model. Simul. Mater. Sci. Eng.* **18** 015012–9